Risk Assessment of Cables Vibration-Suppressed with Tuned-Inerter Dampers

Alin Radu[a,b,*], Irina F. Lazar[a], Simon A. Neild[a], Anastasios Sextos[a,c]

[a] *University of Bristol, Bristol, UK, BS8 1TR*
[b] *Global Parametrics, London UK, EC2Y 9DT*
[c] *Aristotle University of Thessaloniki, Thessaloniki, Greece*

Abstract

This paper has a twofold aim: to assess the performance of tuned-inerter dampers (TIDs) to reduce vibrations in cable structures subjected to seismic ground motions; and to extend an existing TID-design method for cables to a practical scenario of multiple cables in a cable-stayed bridge. In this study, TIDs are installed between the cables and the bridge's deck, the cables being excited at both their ends by the response of the bridge's deck and pylon to seismic ground motions. The seismic hazard is described in a general manner by rates of earthquakes and synthetic ground-motion time histories with respect to their moment magnitudes and epicentral distances. Two approaches that use an existing deterministic method to design TIDs to reduce vibrations in cables are discussed. The first one, perhaps more effective but impractical, assumes that each cable's response is reduced by its own independently-designed TID. The second approach, more realistic and practical, proposes the design of one single TID for all cables to reduce their mid-span response in an optimal way. Numerical results are shown for cable models in the Evripos Bridge in Greece, for which a unique TID is designed for all cables in the bridge, subjected to a hypothetical seismic-hazard scenario. It is shown that the TID-controlled cables have generally a better response, that is a lower average maximum absolute mid-span displacement for most of the cables, and lower variability in the response.

*Corresponding author
Email address: alin.radu@bristol.ac.uk (Alin Radu)

Keywords: Cable structures, Vibration control, Earthquake risk, Tuned-inerter damper, Performance-based engineering, Risk assessment and reduction

1. Introduction

This paper studies the performance of tuned-inerter dampers (TIDs) to reduce seismic vibrarions in cable structures. The use of TIDs in cable structures for seismic-vibration suppression was first introduced by Lazar et al.[1], and this current study extends those findings into a more comprehensive and realistic scenario, that of the cables in a cable-stayed bridge, the Evripos bridge in Greece, described in detail by Sextos et al.[2]. The aim of this study is twofold: (1) to assess the performance of tuned-inerter dampers (TIDs) in the reduction of the seismic-induced vibrations in cables; and (2) to provide a practical framework for selecting a TID design that applies to multiple cables simultaneously, as is needed in the case of a cable-stayed bridge. It must be noted, however, that the research in this paper focuses only on the study of the performance of the uncontrolled and TID-controlled cables. The analysis of the response of the overall bridge on which the cables are installed is beyond the scope of this paper.

Cable-stayed bridges, as with any bridge, are critical parts of infrastructure networks and their damage or failure can result in extensive business interruption as well as significant direct and indirect costs for the affected communities. Thus, accurate risk-assessment and high-performance risk-reduction tools, such as vibration-suppression systems, are important for the preparedness and resilience of critical infrastructure in case of catastrophic events. Even though this paper does not study the overall response of TID-controlled cable-stayed bridges, the reduction of the seismic-induced vibrations in TID-controlled cables is an essential component of this holistic problem [1]. Past research has studied in detail the dynamic behaviour of cables, by determining initially a way to estimate the damping in stay cables using complex-mode analysis [3, 4]. Even

though actions such as wind, fatigue, or temperature may have a higher role on the behaviour of cables, it has been shown that earthquakes may too induce large variations in the internal forces of cables [5], which led previous research to look at various cable layouts in cable-stayed bridges by employing seismic-risk analyses [6]. A comprehensive review on the behaviour of cables subjected to earthquakes [7] also emphasizes the benefits of studying the cable-structure interaction in the seismic response of cable-stayed bridges. Vibration-suppression systems have already been installed between the cables and the deck of cable-stayed bridges to reduce wind-, traffic-, or seismic-induced vibrations [8, 9], and they proved to be efficient. Most of the control systems considered for cables are either viscous dampers [10, 9] or magneto-rheological dampers [11, 12, 13]. Empirical equations for designing the optimum damper-size for simple cables have been developed in previous studies conducted by Yoneda and Maeda [14] and Uno et al.[15]. Applications of semi-active control systems for cables have been discussed in past studies [16, 17]. It has been shown, however, that the effectiveness of the dampers on the reduction of the vibrations in cables has an upper bound [4]. This limitation is due to the location of the damper along the cable, usually constrained within 5% of its length [18] from the connection of the cables to either the deck or the pylon. This constraint may be overcome by replacing the damper with a tuned-mass damper (TMD), which could be located anywhere along the cable's length, as they do not need to be connected to the deck. The TMD's parameters in relation to the cable's inclination and TMD's location on the cable have been studied by Wu and Cai[19]. A further study [20] extended the application of vibration-control of TMDs to shallow cables by adopting a variable-inclination device attached to the cable.

In this study, the tuned-inerter damper (TID), initially developed by Lazar et al. [21], is used as the vibration-control device for the cables. In addition to their use on civi-engineering structures, applications of TIDs have been discussed in several studies [22, 24, 25]. The TID was initially explored as a device that overcomes the aforementioned limitations of a viscous damper[1]. The TIDs, as well as the tuned-mass-damper inerters (TMDIs) [26], incorporate inerters [27],

devices that can generate forces proportional to the relative accelerations between their nodes. TMDIs are similar to TMDs, but with an additional inerter, meant to substitute part of the TMD's mass and connected across two structure attachment-points, like a damper. Unlike the TMDI, the TID substitutes the entire active mass of the TMD through an inerter installed in series with a spring and a damper. Thus, the TID combines the advantages of TMDs used for vibration-control of cables, while preserving the convenience of them being installed near the cables' anchors for easy maintanance access. Other configurations involving inerters, such as tuned viscous-mass damper (TVMDs) [28], have been proposed in the literature —further details are, for example, given in the paper written by Zhang et al.[22]. Alternatively, the use of a new fluid variant of the inerter in enhanced control schemes for civil-engineering structures is presented in a recent study of De Domenico et al. [23].

The current paper expands on the findings of Lazar et el.[1], where a TID was modelled on a cable subjected to harmonic excitation, by considering a more realistic context; namely cables subjected to the response of the deck and the pylons of the Evripos cable-stayed bridge [2], excited via stochastic seismic ground-motions. The bridge is permanently monitored by the EPPO/ITSAK Institution in Thesaloniki and has been the basis of several system identification studies [29, 30] The performance of the TIDs is analysed with respect to different cable geometries, subjected to earthquakes with various frequency contents, characterised by the seismic events' moment magnitudes M and source-to-site distances R. In addition to the analysis of the TID performance with respect to (M, R), the current study also proposes a framework to select one single TID design to fulfil the performance criteria for multiple cables, as is desirable for practical application to a cable-stayed bridge. The paper is structured in three main sections: the first section describes the structural models of the bridge, the cables and the TIDs, as well as the model for the synthetic seismic-ground motions as a function of (M, R); the second section consists of the core risk-assessment and performance-based design of the TIDs for the stay cables; and the third part consists of a numerical evaluation of the TID-controlled cables of

the Evripos bridge subjected to the ground motions in the NGA West database [31].

2. Structural Model and Control System

The goal of this paper is to assess the performance of tuned-inerter dampers (TIDs) installed in cable structures subjected to seismic ground motions. This performance criteria is then used to propose a performance-based framework for the design of TIDs suitable in structures with multiple cables. For the purpose of this study, we will analyse the cables in a cable-stayed bridge. Note again that the study focuses on the response of the cables - the analysis of the overall response of the bridge or of the interdependencies between the responses of the cables and bridge are beyond the scope of this paper.

2.1. Bridge structure and cables layout

The cables from the Evripos Bridge, detailed in the study conducted by Sextos et al.[2], are used as examples for this study. The 136 cables of this bridge are distributed symmetrically about both the longitudinal vertical and the vertical transversal planes of the bridge crossing through the mid-point of the central span. Thus, under the assumption that the response of the bridge is also bisymmetrical with respect to the two planes aforementioned, we only analyse one quarter of the total number of cables. Figure 1(a) shows a simplified model of the left-handed quarter of the bridge considered with the cables numbered from $1-34$. The geometry and finite-element model (FEM) of the Evripos Bridge used for the calibration of our cable models in this study are described in detail in the reference paper by Sextos et al.[2]. It is noted herein that the FE model of the bridge has been updated by means of a multiple-input, multiple-output optimisation and the free-field and on-structure measurements obtained during the 1999 Athens earthquake ($M_w = 6.0$, 7/09/1999), where M_w denotes the moment magnitude of the earthquake.

For the purpose of this study, each cable k is pre-tensioned with a force T_k and is assumed fixed at both ends, that is, one end attached to the pylon, and

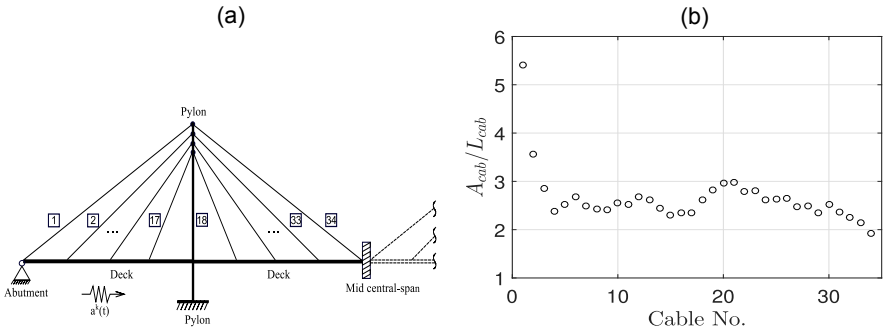

Figure 1: (a) Cable notations and (b) their respective normalized ratios of the cable-cross-section' area to cable's length.

the other end attached to the deck of the bridge. All cables are made of Steel *St*.1670/1860, but have different geometries, briefly summarised in Figure 1(b) using their diameter-to-length normalised ratios. The properties of each cable are shown in Table 1 presented in the Appendix.

2.2. Cable Model

A linear FEM as the one used by Lazar et al.[1] is used to study the response of the cables. Some details of the model are presented in the Appendix, but its full description is available in the citation previously mentioned. The accuracy of the model was validated against the analytical expressions for the combined cable-TID systems using the approach reported for cable-damper systems[4]. The cable is discretized in $N_e = 20$ elements, each of mass m_j, and stiffness $k_j,\ j = 1, ..., N_e$. The displacement response of the cable is characterised by a $(N_e + 1, 1)$ vector $X(t) = \{X_i(t),\ i = 0, ..., N_e\}$, which can be reduced to a $(N_e - 1, 1)$ vector by applying the zero boundary-conditions $X_0 = X_{N_e} = 0$, since the end nodes that connect the cable to the deck and the pylon, respectively, are fixed. Thus, the response of the $N_e - 1$ free nodes is described by the following equation of motion:

$$M\ddot{X}(t) + C\dot{X}(t) + KX(t) = -MA_d(t) + F_{corr}, \tag{1}$$

where a $X(t)$ is the vector of displacements relative to the deck, M, K and C are the mass, stiffness and damping matrices of dimension (N_e-1, N_e-1). The full description of the system's matrices M, K and C for both the controlled and uncontrolled cables is shown in detail in the Appendix.

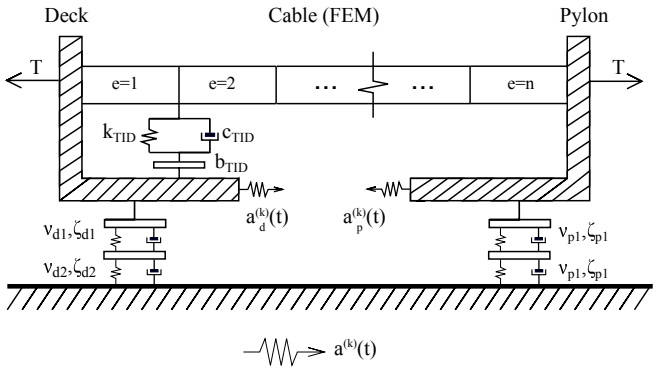

Figure 2: Cable FEM model and surrogate models for the deck's and pylon's responses.

$A_d(t)$ is the response acceleration of the deck to the seismic ground motion $A(t)$ assumed, for the purpose of this study, to be uniform among all pier and abutment supports, and F_{corr} is an excitation force correction vector of dimensions $(N_e-1, 1)$. The vector $F_{corr}(i) = 0$ for $i = 1 \ldots N_e - 2$, while the last element is calculated as a function of the relative displacement response at deck and pylon end of the cable and the stiffness of the cable elements. This correction is necessary due to the fact that the ends of the cables are subjected to different excitations, namely $A_d(t)$ at the deck, and $A_p(t)$ at the pylon. In other words, the ground excitation $A(t)$ is synchronous, but $A_d(t)$ and $A_p(t)$ are asynchronous. These represent the acceleration responses of the deck and pylon, respectively, at the connection with each cable. Sample time can be calculated as samples $a_d^{(k)}(t)$ and $a_p^{(k)}(t)$ of the response accelerations of the bridge FEM to samples $a^{(k)}(t)$ of $A(t)$, as described in the FEM for the Evripos Bridge [2]. However, running the FEM for the bridge to calculate the response of the bridge at the end of the cables for each sample of $A(t)$ is computationally expensive, and thus an approximate method is used to facilitate this calculation. As illus-

trated in Figure 2, two two-degree-of-freedom linear surrogate systems are used to approximate the response of the deck and the pylon to the seismic excitation $A(t)$. The surrogate system approximating the response acceleration $A_d(t)$ of the deck is characterised by four parameters, representing the two modal frequencies (ν_{d1}, ν_{d2}), and the two modal damping ratios (ζ_{d1}, ζ_{d2}) - similarly the surrogate system approximating the response acceleration $A_p(t)$ of the pylon is characterised by the four-parameter vector $(\nu_{p1}, \nu_{p2}, \zeta_{p1}, \zeta_{p2})$. The parameters of the two surrogate models for each cable are estimated such that the differences between the frequency response of the top two peaks of $A_d(t)$ and $A_p(t)$ calculated by the FEM and the surrogate models were minimized.

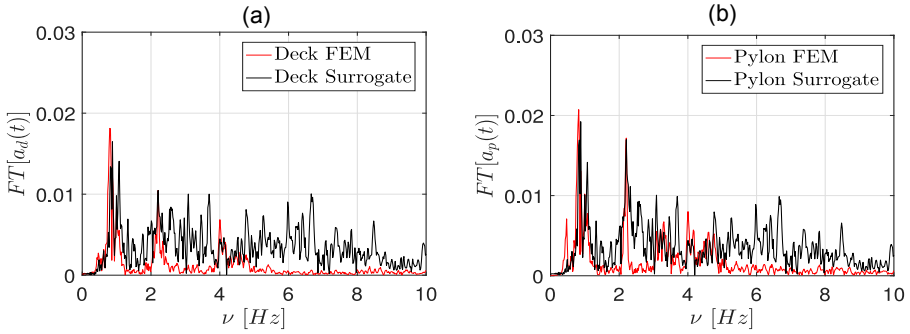

Figure 3: Fourier transforms of the (a) deck's and (b) pylon's responses to the FEM analysis and its surrogate approximate for Cable 9.

Figures 3 (a) and (b) show the Fourier Transform (FT) for the response accelerations $a_d(t)$ and $a_p(t)$ of the deck and pylon, respectively, at the connection points with Cable 9, for both the detailed FEM analysis[2] (red line) and the approximate analysis of the surrogate two-degree-of-freedom models (black lines), for the 1999 Athens earthquake. A similar results is shown in Figure 4 for Cable 22. For all cables it was noticed that the FT transforms presented two dominant peaks, which justifies our decision to use bi-dimensional surrogate models to approximate the bridge's deck and pylon responses.

The calibrated parameters $(\nu_{d1}, \nu_{d2}, \zeta_{d1}, \zeta_{d2})$ characterizing the deck's dynamic response at the connection point with each cable are shown in Figure 5,

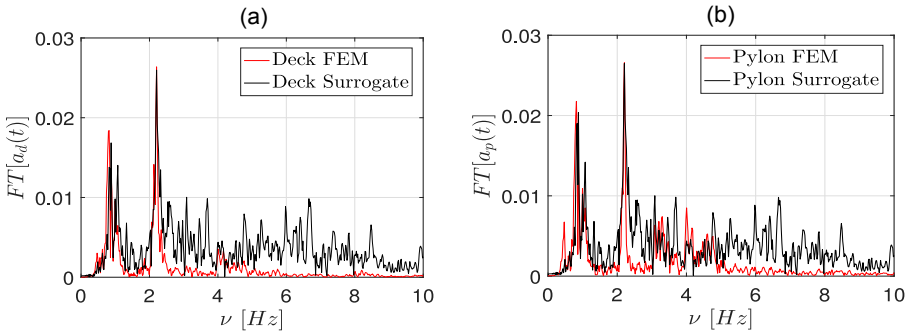

Figure 4: Fourier transforms of the (a) deck's and (b) pylon's responses to the FEM analysis and its surrogate approximate for Cable 22.

while the parameters $(\nu_{p1}, \nu_{p2}, \zeta_{p1}, \zeta_{p2})$ for the pylon's surrogate models at the connection with each cable are shown in Figure 6. The modal frequencies in both cases are approximately constant across all cables, but the damping coefficients vary with respect to each cable. It can be argued that the model used to approximate the response of the bridge is simplistic, but given the scope of the paper to study the behaviour of the cable structures alone, the approximate responses suffice as a good proxy for the excitations at the ends of the cables.

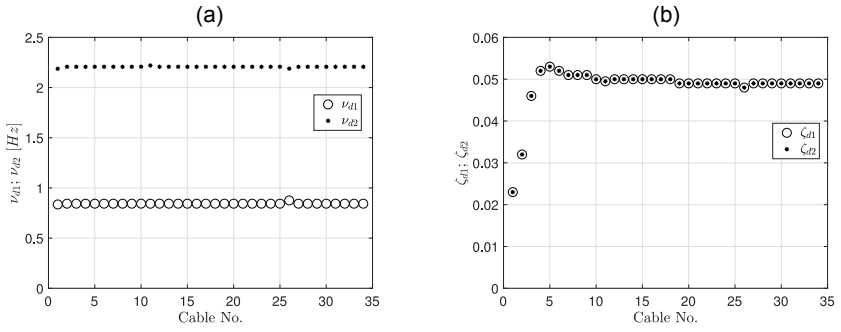

Figure 5: Parameters (a) (ν_{d1}, ν_{d2}) and (b) (ζ_{d1}, ζ_{d2}) for the surrogate models used to approximate the deck's response at the connection with each cable.

2.3. Tuned-Inerter Damper Tuning

TIDs are two-terminal systems that are connected to a structure similarly to dampers. In the case of cables, the TID must be connected between the

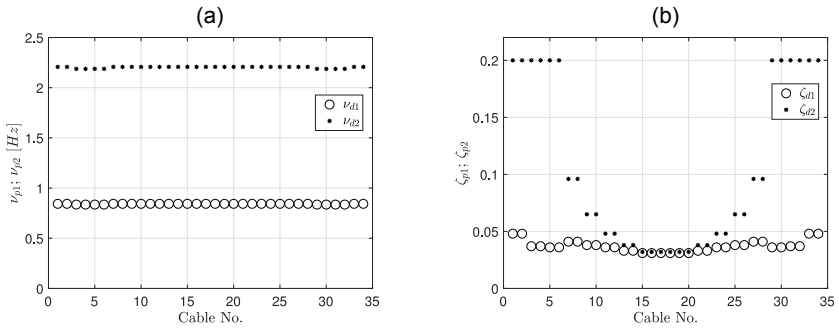

Figure 6: Parameters (a) (ν_{p1}, ν_{p2}) and (b) (ζ_{p1}, ζ_{p2}) for the surrogate models used to approximate the pylon's response at the connection with each cable.

cable and the bridge deck, as shown in Figure 2. For this reason, following the discussion outlined in the original design methodology[1], its connection point is limited between $1\% - 5\%$ of the cables total length L_k, $k = 1 \dots 34$, from the connection of the cable with the deck. It is assumed that the TID's connection point to the cable defines the length of the first element of the cable FEM, i.e. $l_{1,k} \in [0.01, 0.05]L_k$, where $l_{1,k}$ is the distance between the deck support and the TID installation point, measured along a cable's length. As in the case of dampers, the performance of TIDs increases as the connection point is moved further away from the support. For simplicity, in this paper, we assume that the TID is located at 5% of the cable's length, hence for any given cable k, all $N_e = 20$ elements are equal length, i.e. $l_{i,k} = 0.05L_k$, $i = 1, ..., N_e$. Note that the installation of a TID results in the addition of one extra degree of freedom in the equation of motion Eq.(1), for which the dimension of the system will increase from $N_e - 1$ to N_e. The extended versions of the uncontrolled and TID-controlled systems' matrices are provided in the Appendix. The tuning methodology described in [1] uses a deterministic approach based on harmonic oscillations, which will be tested in the risk-analysis section below, by using complex, realistic ground-motions stochastic simulation models. Alternative complex approaches [32, 33] for designing TID-controlled structures subjected to stochastic excitation are also available, and a comprehensive discussion on

the discrepancies of the harmonic-based vs. the stochastic-based approaches is detailed in [33].

The design of the TID for each cable is conducted using the deterministic approach[1], were a number of assumptions were made: (1) the cables were horizontal, (2) the loads at both ends of the cable was identical and (3) the load was a harmonic wave. The TID is fully defined by three parameters: the inertance b_{TID}, that plays the role of the active mass for the system; the stiffness k_{TID}; and damping c_{TID}. The layout of the TID components are shown in Figure 2, and further details on TIDs and their features can be found in the paper that defines this layout for civil-engineering applications [21]. The TIDs parameters can also be translated into three dimensionless parameters, an option adopted in this study: the TID-to-cable mass ratio, $\mu_{TID} = b_{TID}/m_k$, where m_k is the total mass of cable k; the TID frequency of vibration $\nu_{TID} = \sqrt{k_{TID}/b_{TID}}$; and the TID damping ratio $\zeta_{TID} = c_{TID}/(2b_{TID}\nu_{TID})$. Following the guidelines provided by Lazar et al.[1], the tuning of the TID for each cable k is performed in three steps:

Step 1 Set the TID-to-cable mass ratio μ_{TID} and the desired location of the TID, both usually set by the designer, depending on the device limitation or the desired performance level. In this paper, $\mu_{TID} = 0.5$ and the connection point of the TID on the cable is located at $l_{1,k} = 0.05L_k$ along the cable from the cable-deck connection point.

Step 2 Map the $(\mu_{TID}, l_{1,k}/L_k)$ coordinates to find the design cable-to-TID frequency ratio $\rho_{TID} = \nu_{TID}/\nu_k$, where ν_k is the first fundamental frequency of cable k, according to the optimal criteria defined previously[1]. For (0.5,0.05L_k), the corresponding frequency ratio is $\rho_{TID} = 0.915$. Based on ρ, the TID fundamental frequency, νTID can be found for each cable.

Step 3 Map the $(\mu_{TID}, l_{1,k}/L_k)$ coordinates to find the optimal TID damping ratio ζ_{TID}. For (0.5,0.05L_k), the corresponding damping ratio is $\zeta_{TID} = 0.23$.

Two scenarios are considered when designing the TIDs for the bridge. The first, the *idealistic scenario*, is based on the optimal tuning of all 34 TIDs independently, one for each individual cable. The steps described above are applied to obtain the set of optimal parameters (ν_{TID}, ζ_{TID}) for each cable. These will be used to derive the individual TID's stiffness and damping characteristics, which depend on each cable's individual layout and geometry. Note that these designs are optimal in the context set by Lazar et al.[1], of harmonic deterministic loading and they may be suboptimal in the case of the current stochastic ground-motion loads considered in this study. This aspect is discussed in detail in the risk-assessment analysis described in Section 3.1. However, individually specified TIDs for each cable would be expensive and arguably impractical, therefore a second scenario, referred to as the *realistic scenario* is considered. In this scenario a single TID design is selected, from the individual TID designs, that performs best across all 34 cables in some statistical sense (as described in Section 3.2).

2.4. Seismic Input

A cascading approach is adopted to define the input excitation to which the cable structures are subjected, since the cables are not directly subjected to the seismic ground-motions, but rather to the response of the supporting structures, i.e. the deck and the pylon of the bridge that are subjected to the seismic ground-motion. The seismic ground-motions are defined by two components: (1) the distribution of seismic ground-motions with respect to the moment magnitude m and the source-to-site distance r; and (2) the synthetic ground-motion time histories defined as a function of (m, r). Among other parameters, such as the seismic regime, local soil-conditions, the seismic-source parameters (m, r) influence the frequency content of seimsic ground motions, a key component in the dynamic behavior of cables, and structures in general, since their response is sensitive to the frequency content of the excitation [34, 35]. An example of the (m, r)-distribution of earthquakes used for the current study is shown in Figure 7(a). It is for a site in Fresno, California (Lat. = 36.75, Long. = -119.75),

and was obtained using the United States Geological Survey's (USGS) Unified Hazard Tool [36]. The three-dimensional histogram illustrated in Figure 7(a) represents the probability of occurrence $\mathbf{P}(m, r)$ of an earthquake characterized by parameters (m, r).

The model for the synthetic ground-motions used in this study is based on the specific barrier model (SBM) [37, 38], which is a seismological model that provides the frequency content of ground motions as functions of (m, r), in the form of a power-spectral density function $g(\nu; m, r)$ $[m/s^2]$, for fixed local conditions. The SBM was calibrated to global data [39], and can be further updated to a site-specific model as shown by Radu and Grigoriu[40], if local ground-motion record are available.

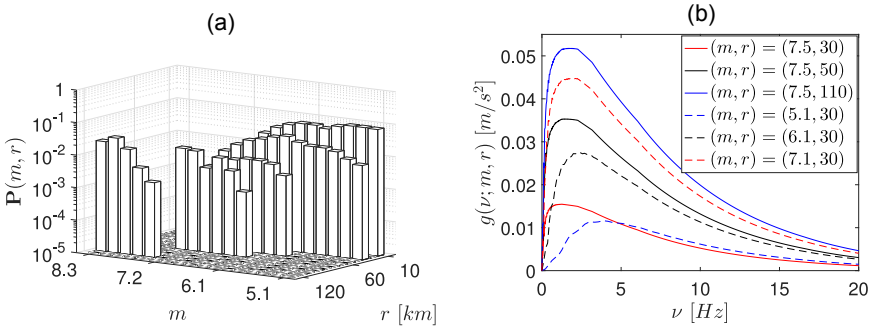

Figure 7: (a) Probability of occurrence $\mathbf{P}(m, r)$, and (b) frequency contents $g(\nu; m, r)$ of seismic ground motions.

Figure 7(b) illustrates the power-spectral density functions $g(\nu; m, r)$ for three pairs of ground motions with fixed moment magnitude $m = 7.5$ and different distances $r \in [30, 50, 110]$ km, and another set of three ground motions with fixed source-to-site distance $r = 30$ km and magnitudes $m \in [5.1, 6.1, 7.1]$. This plot demonstrates the motivation behind this study focusing on the risk assessment of TID-controlled cables on different types of earthquakes distributed by (m, r), namely that these parameters are significant contributors on the frequency contents of ground motions. More details on this argument are provided in previous studies[34, 41]. It must be noted that the above distribution

of events by (m, r), even though defined for specific location, can be replaced with a distribution from a more detailed probabilistic seismic-hazard analysis (PSHA). The use of this (m, r) distribution in this paper is aimed to generate ground motions with a wide range of frequency content in order to demonstrate the efficiency of TIDs. The seismic ground-motions are assumed to be samples of a non-stationary, non-Gaussian stochastic process $A(t)$ with finite duration t_f:

$$A(t) = h(t)Z(t),\ 0 \leq t \leq t_f, \tag{2}$$

where $h(t) = \alpha t^{\beta} \exp\{-\gamma t\}$ is a deterministic amplitude-modulation function with constant (m, r)-dependent parameters α, β and γ, that are also outputs of the SBM; and $Z(t)$ is a zero-mean, stationary, process with a generalized Student's T marginal distribution, calibrated to account for a kurtosis coefficient of 14.3 that corresponds to type-C NEHRP soil [42]. The use of a non-Gaussian distribution for the process $A(t)$, allows to capture the local site amplification of ground motions, reflected in a kurtosis coefficient higher than 3, the typical value for Gaussian process. Details about this model and its calibration can be found in the study conducted by Radu and Grigoiru[42]. However, other stochastic [43, 44, 45] or physics-based [46] models for synthetic ground motions can be used in place of the model in Eq.(2). Samples of the process $A(t)$ are simulated using the spectral representation method[47], used before for this purpose by Deodatis[48]. A total number of $1,000$ $A(t)$ samples for each pair of (m, r) relevant for the site selected was used in the analysis.

3. Risk Assessment and Performance-based Design

The risk assessment and the framework proposed for the design of the TIDs for the cable structures are performed with respect to the mid-span transversal displacement of the cable, i.e. $X_m = X_{N_e/2}$ in Eq. (1), where N_e is assumed to be an even number of elements used for the cable FEM, and $N_e = 20$ for this particular case study. Note that other measures of performance can be used

in the discussion herein, such as the use of more complex metrics for seismic-reliability analyses - see [49] for example.

3.1. Idealistic Scenario

In the idealistic scenario, the TIDs would be customised for each individual cable. The methodology used for the design of TIDs for cable structures is briefly described in Section 2.3 with references to the Appendix, and presented in detail in the original paper of Lazar et al.[1]. In this scenario, sets of the three parameters $(b_{TID}, \nu_{TID}, \zeta_{TID})$ defining the TID are designed for each cable using the approach aforementioned. The response performance of the cables is quantified by a two-dimensional fragility function, i.e. the probability of the mid-span displacement X_m exceeding a given custom critical value x_{cr}, for a given earthquake characterised by (m, r):

$$P_f(m, r) = \mathbf{P}\{X_m > x_{cr} | (M, R) = (m, r)\}. \tag{3}$$

We will refer to the graphical representation of $P_f(m, r)$ as fragility surfaces[34]. Note that the fragility function $P_f(m, r)$ is calculated in the (m, r) space since the response of the cables is sensitive to the frequency of the seismic ground-motion, and their frequency contents is dependent on (m, r) among other parameters, as shown in Figure 7(b). Panels (a) of Figures 8 and 9 show the fragility surfaces for the Cables 9 and 22, respectively, without a TID installed, for $x_{cr} = 1.0m$ (approx. 2% of the average cable length). Panels (b) of Figures 8 and 9 show the corresponding $P_f(m, r)$ that reflect the effect of the TIDs installed in each cable.

The probabilities $P_f(m, r)$ are expected to be smaller in the case of the TID-controlled cables than the uncontrolled case. Figures 8 and 9 show, however, that the effects of the TIDs on the cable responses can be different even though the TIDs are designed using the same approach. Specifically, the TID is more likely to reduce the mid-span response in Cable 9 than in Cable 22, as the fragility surface for Cable 9 reduces significantly towards zero values, while the surface for for Cable 22 reduces just slightly, resembling more the surface for

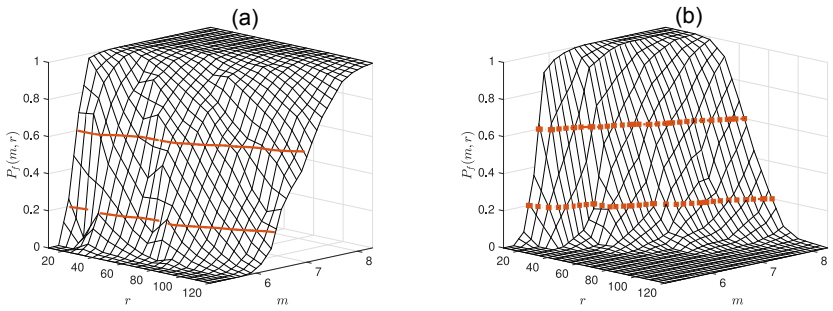

Figure 8: Fragility surface for the (a) uncontrolled and (b) TID-controlled mid-span response of Cable 9.

the uncontrolled cable. For example, in the case of Cable 9, the probabilities of the mid-span displacement to exceed x_{cr} for earthquakes of magnitude $m = 8$, are reduced from almost 1 for the uncontrolled cable to almost 0 for the TID-equipped cable, for source-to-site distances $r \in [100, 120]$ km. For the same range of (m, r), the probabilities of exceeding x_{cr} for Cable 22 stay the same or get reduced to a third of the values for the uncontrolled cables. This result is not surprising, but suggests that the deterministic approach used for the design of the TIDs may lead to sub-optimal designs when the cables are subjected to inputs with a large spectrum of frequency contents, as in the current study. This effect is seen more clearly in Figure 10, which shows cross-sections through the surfaces in Figures 8 and 9, for a fixed value $r = 40$ km, i.e. $P_f(m, 40km)$ for the uncontrolled and the TID-controlled Cables 9 and 22, respectively .

For a broader overview of the performance of the cable structures along the bridge, Figure 11 shows contours of the fragility surfaces for eight uncontrolled (solid lines) and TID-controlled (dashed lines) cables throughout the section of the bridge analysed (Cables 5, 7, 9, 11, 20, 22, 24, 26) calculated for two levels (a) $P_f(m, r) = 0.2$, and (b) $P_f(m, r) = 0.6$. In other words, these figures show horizontal cross-sections through the fragility surfaces for each of those cables at the two specified $P_f(m, r)$ levels. Note the colour of the cable numbers match the colours of the corresponding curves. The areas to the upper-left part of the curve indicate the range of (m, r) values for which the level of the $P_f(m, r)$ specified

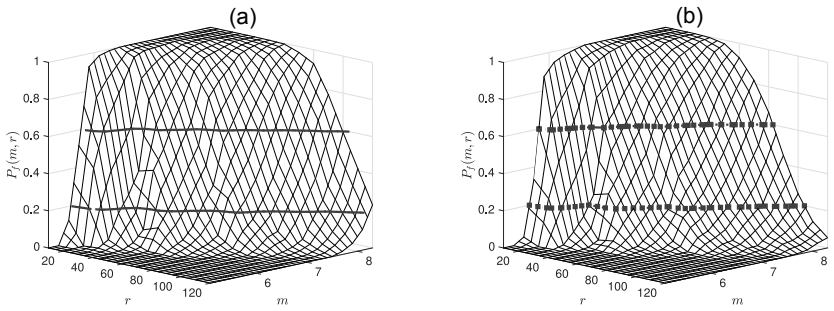

Figure 9: Fragility surface for the (a) uncontrolled and (b) TID-controlled mid-span response of Cable 22.

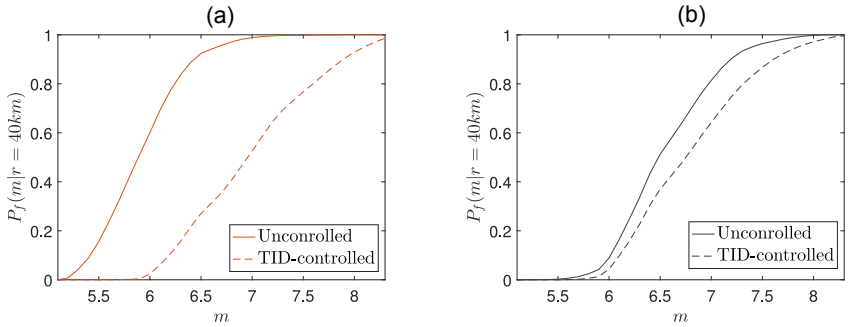

Figure 10: Probability $P_f(m, 40km)$ for the uncontrolled (solid line) and the TID-controlled (dashed line) for (a) Cable 9 and (b) Cable 22.

is exceeded. Thus, the more the dashed line is shifted to the upper-left of the solid line with the same colour, the more the TID improves the performance of that specific cable. Consistent with Figures 8 and 9, Figure 11 shows that Cable 9 performs significantly better than Cable 22 when a TID is present. For example, focusing on Cable 11, and probability of failure equal to $P_f = 0.2$, the TID-equipped cables can resist a $m = 7$ earthquake event occurring at a distance $r = 27\ km$, where as the standard (non-TID) cables have the same probabilistic performance for $m = 7$ and $r = 42\ km$. In other words, based on a commonly used ground-motion prediction equation, such as the one developed by Boore et al.[50], the uncontrolled Cable 11 performs similarly to the same TID-equipped cable subjected to a ground-motion acceleration of greater by

approximately 42%.

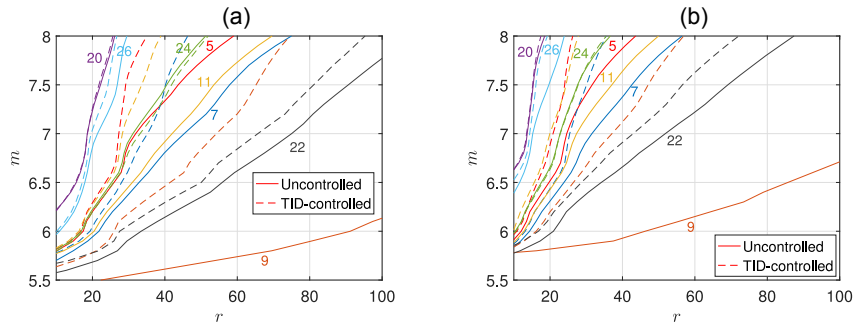

Figure 11: Fragility-surface contour at (a) $P_f = 0.2$ and (b) $P_f = 0.6$ for the uncontrolled (solid lines) and TID-controlled (dashed lines) for Cables 5, 7, 9, 11, 20, 22, 24 and 26.

A closer look at Figure 11, shows that for some cables, such as Cable 24 or 20, the TID brings little or no benefits to the cable response or can have a slight opposite effect. Despite the adopted deterministic design method for TIDs being effective in almost all cases, this risk-assessment of their performance demonstrates optimisation limitations which may lead to undesired results.

3.2. Realistic Scenario

In a realistic scenario, it is desirable that only a limited number of TIDs designs would be used across the cables over a cable-stayed bridge. Thus, we now explore the more practical case in which a single TID design is installed across all 34 cables. This unique TID is selected from the 34 TIDs designed in the previous Section 3.1, by considering the performance across all cables. The performance criterion is defined with respect to the tail probability distribution of maximum absolute mid-span displacement of the cable compiled for all types of earthquakes in the seismic-hazard scenario considered, that is,

$$F(x) = \sum_{m,r} \mathbf{P}(\max_{t\geq 0} |X_m(t)| > x | (M,R) = (m,r)) \mathbf{P}(m,r), \tag{4}$$

where $\sum_{m,r}$ indicates the summation over the entire range of (m,r) for which $\mathbf{P}(m,r)$ is available, as shown in Figure 7(a). In other words, $F(x)$ in Eq.(4) is

the average of the exceedance probabilities calculated in Eq.(3) for a range of critical value $x_{cr} = x$, weighted by the occurrence probabilities $\mathbf{P}(m, r)$ for each earthquake.

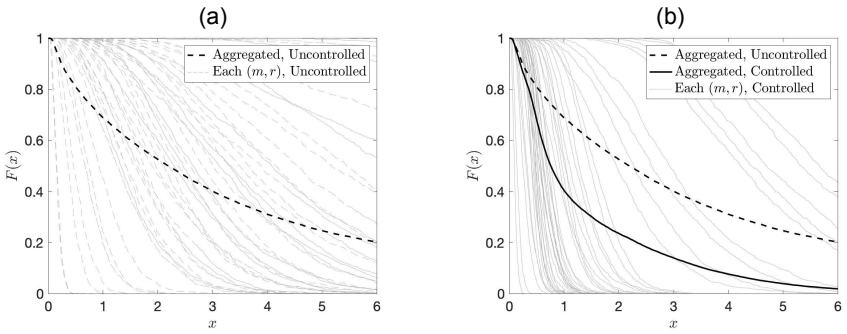

Figure 12: Probability-of-exceedance curves for the (a) uncontrolled and the (b) TID-controlled Cable 9.

Considering the TIDs designed for cables 9 and 22, Figures 12 and 13 show in grey lines the exceedance probabilities in Eq.(3) for each pair (m, r) for a range of $x_{cr} = x$ up to $6m$ for (a) the uncontrolled and (b) the TID-controlled cables, in dashed and solid lines, respectively. The black bold lines illustrate the average tail probabilities $F(x)$ in Eq.(4). Note that the function $F(x)$ for the uncontrolled line in panel (a) represented in dashed line is carried over in panel (b) for the TID-controlled case, for comparison.

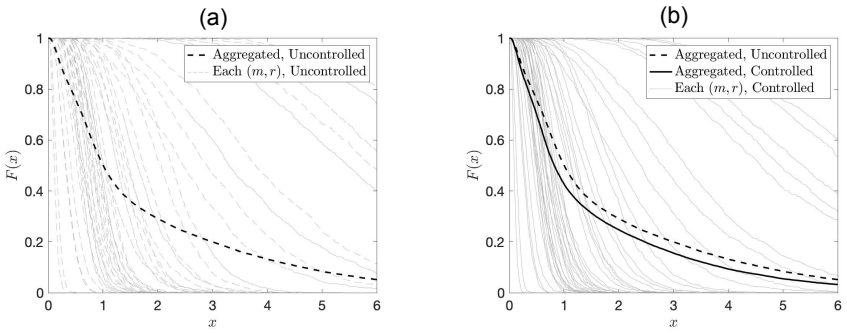

Figure 13: Probability-of-exceedance curves for the (a) uncontrolled and the (b) TID-controlled Cable 22.

In line with the fragility surfaces in Figures 8 and 9, the TID performs better overall for Cable 9 than for Cable 22. These exceedance probability curves in Eq.(4) are now calculated for all cables in the bridge and are indexed by $k = 1, ..., 34$. Then, the following quantity, gain Γ_k, is calculated:

$$\Gamma_k = \int_x \left(F_k(x) - F_k^{TID}(x) \right) dx, \tag{5}$$

where $F_k(x)$ and $F_k^{TID}(x)$ are calculated as shown in Eq.(4) for the uncontrolled and TID-controlled cable k for a range of critical values x. If gain $\Gamma_k < 0$, then the presence of the TID is deleterious to the cable performance, i.e. the TID-controlled cable is more likely to produce a higher (i.e. detrimental) response than the uncontrolled cable. If gain $\Gamma_k > 0$, then the response of the TID-controlled cable is more likely to be reduced compared to the response of the uncontrolled cable, and a higher value of Γ_k indicates a better performance of the TID.

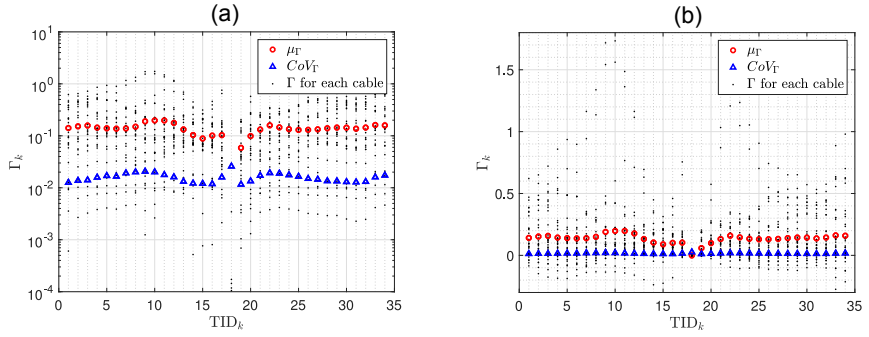

Figure 14: Cable gains Γ_k and their means and coefficient of variations calculated for each TID$_k$.

Figure 14 shows with black dots on (a) logarithmic and (b) linear scales, the gain values Γ_k calculated for each cable k controlled by each of the 34 TIDs designed in Section 3.1, denoted by TID_k . These plots are arranged to show the gains for each TID over the entire range of cables in order to summarize the performance of each TID, which would help in the selection process of one unique device for all cables. The red-circular and blue-triangular markers indicate the mean ν_Γ and the coefficients of variation CoV_Γ for the gains calculated for each

TID over the entire range of cables. Note that while the logarithmic-scale plot shows the level of performance of each TID clearly, it does not highlight the negative values of the gain, see the linear plot for these. We set as the selection criteria of the TID for the entire bridge, the maximum ν_Γ and the minimum CoV_Γ. These criteria are satisfied by TID_{11}, i.e. the TID designed for Cable 11 in Section 3.1, and ensures the best mean gain over all cables, with the least variability around it. By looking at Figure 14(b) it can be noticed that TID_{11} would generate negative gain for some cables, hence for these the TID should not be installed. If the selection criterion is to choose a TID that produces the minimum number of negative gains, then TID_{19} would be a better choice. Of course, the selection of the TID will ultimately be based on the engineering judgement and it could also involve the possibility of selecting more than one TID for the cables on the bridge, as well as the option of not installing any TID for some cables. However, such a decision analysis is beyond the scope of our paper, in which we just propose the framework for such a discussion.

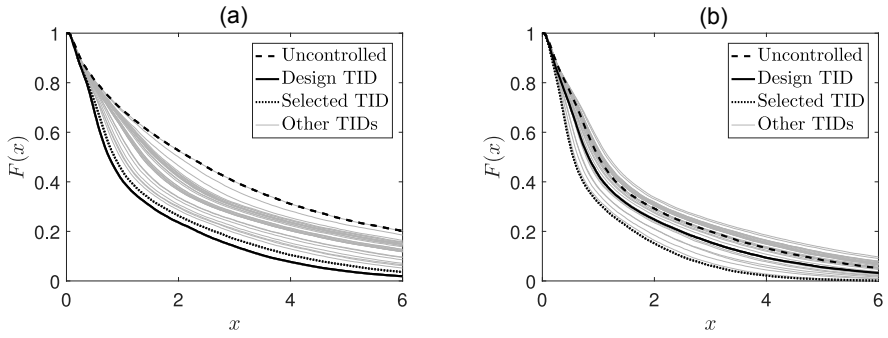

Figure 15: Probability-of-exceedance curves for the design and overall-selected TIDs for (a) Cables 9 and (b) Cable 22.

Figure 15 shows the exceedance-probability curves for the previously analysed Cables 9 and 22, for the uncontrolled responses (dashed line), for the controlled responses with the corresponding TIDs designed in Section 3.1 (solid line), for the controlled responses with the selected TID_{11} (dotted line), and the controlled responses with the other TIDs designed for the other cables on

the bridge. It can be seen that while the selected TID performs slightly poorer for Cable 9 than its corresponding designed TID_9, in case of Cable 22, the performance of the selected TID_{11} is considerably better than its corresponding design TID_{22}. Note that the *selected TID* refers to the unique TID selected as the "best" controlling device for all cables, while the *design TID* refers to the individually designed TID for each cable. Based on the above criteria set in Figure 14 and observations made for these two particular cables it can be seen that the TID designed for Cable 11 is a an overall good choice.

4. Numerical Results and Discussion

Based on the analysis done in Section 3.2, the TID designed for Cable 11 was chosen as the unique TID to be installed for all cables on the bridge, based on the established criteria. To test the performance of the selected TID_{11} for each cable to real ground-motion records, the mid-span uncontrolled and TID-controlled responses for each cable are calculated for approximately $3,500$ records in the NGA-West dataset [31]. Figure 16 shows the NGA-West empirical tail probability-distribution functions of the mid-span responses for each of the 34 uncontrolled and controlled cables with the selected TID_{11}. In the same figure, the black circles mark the mean absolute maximum mid-span displacements of each cable, which are reduced in the controlled cables, in most of the cases.

However, the biggest advantage of the TID is that the variability in the response is reduced, shown clearly in Figure 17, which is a summary of the first two statistical moments of the distributions in Figure 16. This figure shows the means and the coefficients of variation, i.e. standard deviations normalized by the means, for each cable's distributions of the maximum absolute displacements. In general, the average displacements in the cables are reduced —e.g. in Cables 9 and 22, from 0.63 m to 0.19 m, and from 0.23 m to 0.11 m, respectively—, but the bigger gains are in the reduction of the uncertainties of the maximum displacements —e.g. the coefficients of variation in Cables 9 and 22,

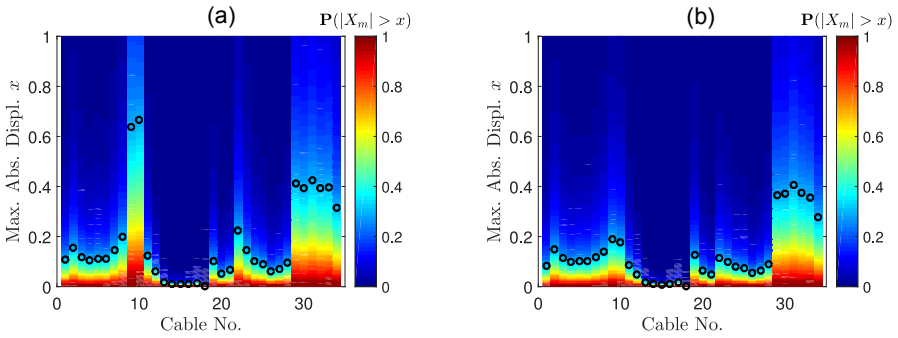

Figure 16: Empirical cumulative-distribution functions for the maximum absolute displacements calculated from the NGA-West data of the (a) uncontrolled and (b) selected-TID-controlled responses for each cable.

are reduced to less than a third from 65% to 20%, and to a half from 68% to 34%, respectively.

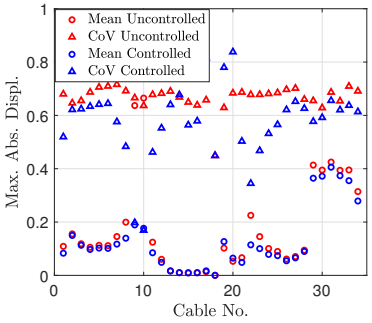

Figure 17: Means and coefficient of variations (CoV) for the empirical distributions of the maximum absolute displacements in Figure 16.

Figure 18 shows the probability density functions of the mid-span maxi-
420 mum absolute displacements for the uncontrolled and TID-controlled Cables 9 and 22. It can be seen that, even though the mean responses have not been shifted significantly, the tails of the distributions are lighter. This achievement is important because it demonstrates that there is a lower probability of having extreme values, and thus, the TID manages to reduce large values of the
425 response in the cables.

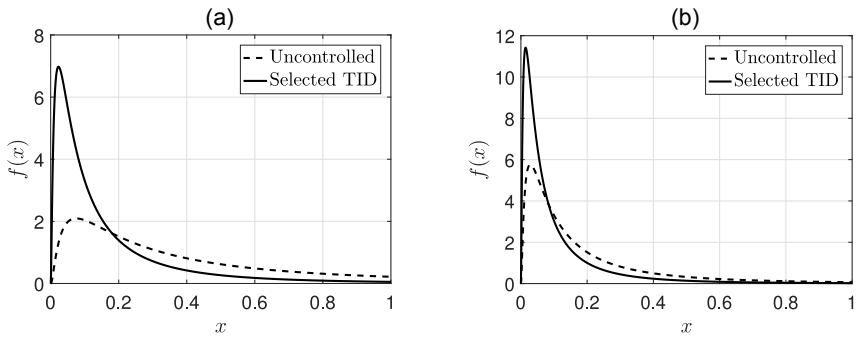

Figure 18: Probability-density functions for the maximum absolute displacements fitted to the NGA-West-data uncontrolled and selected-TID-controlled responses for (a) Cable 9 and (b) Cable 22.

5. Conclusions

The current paper assessed probabilistically the performance of tuned-inerter dampers (TIDs) installed in cable structures subjected to seismic loads, and proposed a performance-based framework to select TIDs that satisfy simultaneously the response of multiple independent cables. The cables analysed in this study are part of a cable-stayed bridge and are installed between the deck and the pylon of the bridge, which is subjected to seismic loads. The current research focused only on the analysis of the cables, and simple surrogate models were used to estimate the response of the deck and pylon of the bridge. Numerical results are shown for cable models in the Evripos Bridge in Greece, subjected to a hypothetical seismic-hazard scenario, as well as for the real ground-motion records in the NGA-West earthquake database.

A comprehensive reliability analysis was employed to study the performance of TIDs installed in the bridge's cables, subjected to synthetic ground-motion records with various frequency contents characterised by their moment magnitudes and source-to-site distances, as well as other factors such as local soil conditions or seismic regime. The TIDs were designed using a classical deterministic approach developed, and the aim was to quantify the performance of such-designed TIDs as well as extend this method into a performance-based de-

sign approach. Fragility surfaces as functions of moment magnitude and source-to-site distance were developed for the uncontrolled and TID-controlled cables. Two performance-based design approaches were analysed in this study: one idealistic in which each cable had its own customised (and individually optimised) TID, and one more practical in which one single TID was selected for all bridge's cables.

The results have shown that even in the practical case of performance-based design of one single TID to reduce optimally the response in multiple cables, the reductions across all cables can still be significant, of up to 2-4% of the original response at extremes, and sometimes outperform the optimal deterministic design. Also, lighter tails observed in the response of the TID-controlled cables indicate a lower likelihood of extreme response, which makes this solution attractive for extreme loads, such as in the case of strong earthquakes. There are indeed exceptions, such as when certain TID designs amplify the response of cables for inputs of some specific frequency contents, but the overall trend of using TIDs is beneficial and has shown their potential in case of seismic loads. Further research is needed particularly in relation to the definition of one single best cable to be optimized, the response of the cables under actual, recorded earthquake ground motions and the life-cycle cost of TIDs, including the determination of cables that would not need such a system implemented.

Appendix

Finite Element Model

In order to reduce computational effort, a finite element model of the cable was created using axial elements[1] . The axial elements are pinned at both ends and act as springs, allowing displacement of both ends. This type of element is generally used for modelling cables and can only support axial loading [51, 52].

Following common practice, for each element, we can write a force-displacement relationship. In the case of cable elements, the stiffness of each element will be $k_i = T/l_{ei}$, where k_i and l_{ei} are the stiffness and length of element i respectively

and T is the tension in the cable. Stiffness and mass matrices can be written for each axial element, which are then assembled to form the stiffness and mass matrix of the cable. Therefore, for a cable divided into n elements and fixed at both ends

$$\mathbf{K} = \begin{bmatrix} k_1 + k_2 & -k_2 & 0 & \dots & 0 & 0 \\ -k_2 & k_2 + k_3 & -k_3 & \dots & 0 & 0 \\ \vdots & \vdots & \vdots & \vdots & \vdots & \vdots \\ 0 & 0 & 0 & \dots & k_{N_e-1} + k_{n-1} & -k_{N_e-1} \\ 0 & 0 & 0 & \dots & -k_{N_e-1} & k_{N_e-1} + k_{N_e} \end{bmatrix}, \quad (6)$$

and

$$\mathbf{M} = \frac{1}{6} \begin{bmatrix} 2m_1 + 2m_2 & m_2 & 0 & \dots & 0 & 0 \\ m_2 & 2m_2 + 2m_3 & m_3 & \dots & 0 & 0 \\ \vdots & \vdots & \vdots & \vdots & \vdots & \vdots \\ 0 & 0 & 0 & \dots & 2m_{N_e-2} + 2m_{N_e-1} & m_{N_e-1} \\ 0 & 0 & 0 & \dots & m_{N_e-1} & 2m_{N_e-1} + 2m_{N_e} \end{bmatrix}. \quad (7)$$

The necessary number of finite elements was chosen to ensure a good level of accuracy. For this, compared the first natural frequency of the finite element modelled cable to the one calculated using the analytical formula $\omega_c = \pi/L\sqrt{T/m}$. The model with $N_e = 20$ elements was chosen, as the percentage error is approximately 0.1%. Since cables have very low inherent damping, we considered $C = 0$. All numerical values defining the cables' parameters are given in Table 1. More details on this procedure are given in the Appendix of [1].

For the TID-controlled system, the mass M, damping C, and stiffness K matrices in the equation of motion Eq. (1) are replaced by $M^{(d)}$, $C^{(d)}$ and $K^{(d)}$ of the structural system equipped with the TID. Note that the new matrices for the TID-controlled structure have $N_e+1 = 21$ degrees of freedom, the additional one being introduced by the TID. For a better understanding of how the TID affects the behaviour of the host structure, the matrix forms of $M^{(d)}$, $C^{(d)}$ and

$K^{(d)}$ are provided below as functions of the original mass, damping and stiffness matrices M, C and K:

$$M^{(d)} = \begin{pmatrix} & & & 0 \\ & \left(M\right) & & 0 \\ & & & \vdots \\ & & & 0 \\ 0 & 0 & \dots & m_d \end{pmatrix},$$

$$C^{(d)} = \begin{pmatrix} c_d & 0 & \dots & 0 & -c_d \\ 0 & & & & 0 \\ \vdots & & \left(O_{N_e-1}\right) & & \vdots \\ 0 & & & & 0 \\ -c_d & 0 & \dots & 0 & c_d \end{pmatrix} + \begin{pmatrix} & & & & 0 \\ & & \left(C\right) & & 0 \\ & & & & \vdots \\ & & & & 0 \\ 0 & 0 & \dots & 0 & 0 \end{pmatrix}.$$

The updated stiffness matrix has the same layout as $C^{(d)}$, where c_d is replaced by k_d and C is replaced by K.

$$K^{(d)} = \begin{pmatrix} k_d & 0 & \dots & 0 & -k_d \\ 0 & & & & 0 \\ \vdots & & \left(0_{N_e-1}\right) & & \vdots \\ 0 & & & & 0 \\ -k_d & 0 & \dots & 0 & k_d \end{pmatrix} + \begin{pmatrix} & & & & 0 \\ & & \left(K\right) & & 0 \\ & & & & \vdots \\ & & & & 0 \\ 0 & 0 & \dots & 0 & 0 \end{pmatrix},$$

where O_{N_e-1} is a zero square matrix of dimension $N_{dof}-1$. The construction of matrices $M^{(d)}$, $C^{(d)}$ and $K^{(d)}$ requires the use of the TID parameters b_{TID}, c_{TID} and k_{TID} (as defined in the main body of the paper). The TID is connected at $l_{1,k} = 0.05L_k$, between the deck and cable.

TID tuning

The TID is tuned based on the study by Lazar et al.[1], where the optimisation criterion is the minimisation of the cable midspan displacement when the

cable is subjected to harmonic excitation. Note that the criterion for the tuning of the TIDs was chosen to be consistent with the original study in [1], but any other objective function may be used, given the flexibility offered by the full dynamic analysis of the cables' behaviours. Once the cable's mass ratio and connection point are set as detailed in Section 2.3, the designer can look up the corresponding frequency ratio, ρ_{TID} and damping ratio, ζ_{TID}, using Figure 19.

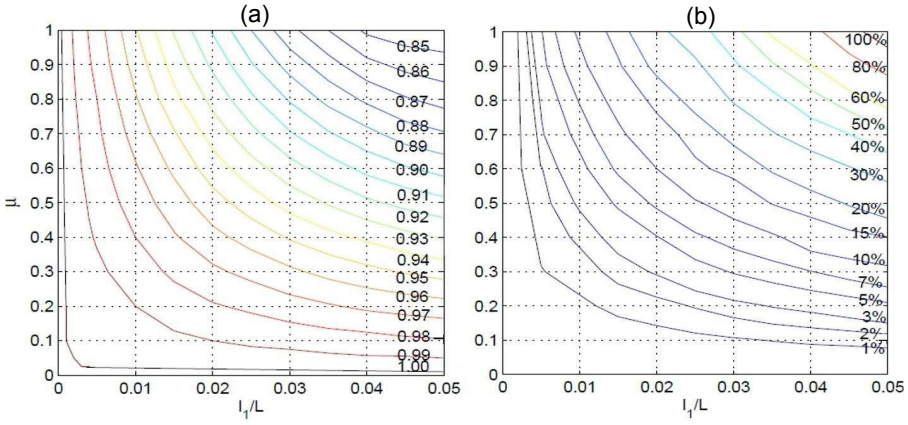

Figure 19: Contour plots for determining the optimal TID parameters as a function of the mass and length ratio from [1]: (a) plot used to determine the cable-to-TID optimal frequency ratio (ρ_{TID}); (b) plot used to determine the optimal TID damping ratio (ζ_{TID}).

For example, for the case considered in this paper, where $\mu_{TID} = 0.5$ and $l_{1,k} = 0.05L_k$, the resulting values extracted from Figure 19 are $\rho_{TID} = 0.915$ and $\zeta_{TID} = 0.23$, as already mentioned in Section 2.3. Using the data in Table 1 and the expressions given in Section 2.3, the TID parameters can be evaluated for each cable. The data related to the geometry of all 34 cables analysed in this paper is presented in Table 1.

Compliance with Ethical Standards

Funding: A.R. was funded by the Marie Skłodowska-Curie Actions of the European Union's Horizon 2020 Program under the Grant Agreement No. 704679 - PARTNER. S.A.N. was funded by the EPSRC Fellowship EP/K005375/1.

Table 1: Cable Properties.

k	$T_k[kN]$	$A_k[cm^2]$	$L_k[m]$	k	$T_k[kN]$	$A_k[cm^2]$	$L_k[m]$
1	1044.1	56	103.6	18	53	11.2	42.86
2	1193.9	35.2	98.7	19	74	12.6	44.75
3	1217.1	26.6	93.18	20	237.3	14	47.32
4	1218.8	21	88.47	21	431.5	15.4	51.6
5	1195.1	21	83.04	22	583.6	15.4	55.08
6	1010.1	21	78.53	23	683.9	16.8	59.98
7	1020.6	18.2	73.26	24	692.9	16.8	64.07
8	940.4	16.8	69.03	25	759	18.2	69.33
9	931	15.4	64	26	744.2	19.6	73.81
10	860.3	15.4	60.18	27	792.4	19.6	79.3
11	797.7	14	55.52	28	818.9	21	84.06
12	794.2	14	52.28	29	901.2	21	89.7
13	731.4	12.6	48.22	30	837.7	23.8	94.64
14	708.3	11.2	45.86	31	793.4	23.8	100.38
15	602.4	9.8	42.73	32	963.3	23.8	105.47
16	417.8	9.8	41.6	33	2031.1	23.8	111.27
17	176.5	9.8	41.63	34	2409	22.4	116.46

Conflict of Interest: The authors declare that they have no conflict of interest.

References

[1] I.F. Lazar, S.A. Neild, and D.J. Wagg, "Vibration suppression of cables using tuned inerter dampers," *Engineering Structures*, vol. 122, pp. 62 – 71, 2016.

[2] A. Sextos, C. Karakostas, V. Lekidis, and S. Papadopoulos, "Multiple support seismic excitation of the evripos bridge based on free-field and on-structure recordings," *Structure and Infrastructure Engineering*, vol. 11, no. 11, pp. 1510–1523, 2015.

[3] B. M. Pacheco, Y. Fujino, and A. Sulekh, "Estimation curve for modal damping in stay cables with viscous damper," *Journal of Structural Engineering*, vol. 119, no. 6, pp. 1961–1979, 1993.

[4] S. Krenk, "Vibrations of a taut cable with an external damper," *ASME Journal of Applied Mechanics*, vol. 67, no. 4, pp. 772–776, 2000.

[5] J. Yi and J. Li, "Longitudinal Seismic Behavior of a Single-Tower Cable-Stayed Bridge Subjected to Near-Field Earthquakes," *Hindawi Shock and Vibration*, https://doi.org/10.1155/2017/1675982, 2017.

[6] V.A. Noghabi and K. Bargi, "Study on Different Cable Configurations of Cable-Stayed Bridges Using Developed Seismic Risk Assessment," *Structural Engineering International*, vol. 26, no. 4, pp. 312–323, DOI: 10.2749/101686616X14555428759280, 2016.

[7] A. Camara, "Seismic behavior of cable-stayed bridges: a review," *MOJ Civil Eng.*, vol. 4, no. 3, pp. 161–169, DOI: 10.15406/mojce.2018.04.00115, 2018.

[8] J. A. Main and N. P. Jones, "Evaluation of viscous dampers for stay-cable vibration mitigation," *Journal of Bridge Engineering*, vol. 6, no. 6, pp. 385–397, 2001.

[9] Y. Fujino and N. Hoang, "Design formulas for damping of a stay cable with a damper," *Journal of Structural Engineering*, vol. 134, no. 2, pp. 269–278, 2008.

[10] Y. L. Xu and Z. Yu, "Vibration of inclined sag cables with oil dampers in cable-stayed bridges," *Journal of Bridge Engineering*, vol. 3, no. 4, pp. 194–203, 1998.

[11] H.-J. Jung, B. F. Spencer, and I.-W. Lee, "Control of seismically excited cable-stayed bridge employing magnetorheological fluid dampers," *Journal of Structural Engineering*, vol. 129, no. 7, pp. 873–883, 2003.

[12] F. Weber, G. Feltrin, and M. Motavalli, "Passive damping of cables with mr dampers," *Materials and Structures*, vol. 38, pp. 568–577, Jun 2005.

[13] M. Liu, G. Song, and H. Li, "Non-model-based semi-active vibration suppression of stay cables using magneto-rheological fluid dampers," *Smart Materials and Structures*, vol. 16, no. 4, p. 1447, 2007.

[14] M. Yoneda and K.-i. Maeda, "A study on practical estimation method for structural damping of stay cables with dampers," *Doboku Gakkai Ronbunshu*, vol. 1989, no. 410, pp. 455–458, 1989.

[15] K. Uno, S. Kitagawa, H. Tsutsumi, A. Inoue, and S. Nakaya, "A simple method of designing cable vibration dampers of cable-stayed bridges," *J. Struct. Engrg*, vol. 37, 1991.

[16] A. K. Agrawal, J. N. Yang, and W. L. He, "Applications of some semiactive control systems to benchmark cable-stayed bridge," *Journal of Structural Engineering*, vol. 129, no. 7, pp. 884–894, 2003.

[17] E. A. Johnson, G. A. Baker, B. Spencer Jr, and Y. Fujino, "Semiactive damping of stay cables," *Journal of Engineering Mechanics*, vol. 133, no. 1, pp. 1–11, 2007.

[18] C. S. Cai, W. J. Wu, and X. M. Shi, "Cable vibration reduction with a hung-on tmd system. part i: Theoretical study," *Journal of Vibration and Control*, vol. 12, no. 7, pp. 801–814, 2006.

[19] W. J. Wu and C. S. Cai, "Cable vibration reduction with a hung-on tmd system, part ii: Parametric study," *Journal of Vibration and Control*, vol. 12, no. 8, pp. 881–899, 2006.

[20] F. Casciati and F. Ubertini, "Nonlinear vibration of shallow cables with semiactive tuned mass damper," *Nonlinear Dynamics*, vol. 53, pp. 89–106, Jul 2008.

[21] I. F. Lazar, S.A. Neild, and D.J. Wagg, "Using an inerter-based device for structural vibration suppression," *Earthquake Engineering and Structural Dynamics*, vol. 43, no. 8, pp. 1129–1147, 2014.

[22] S. Zhang, J. Jiang, and S. Neild, "Optimal configurations for a linear vibration suppression device in a multi-storey building," *Structural Control and Health Monitoring*, vol. 24, no. 3, pp. 1–17, 2017.

[23] D. De Domenico, P. Deastra, G. Ricciardi, N.D. Sims, and D.J. Wagg, "Novel fluid inerter based tuned mass dampers for optimised structural control of base-isolated buildings," *Journal of the Franklin Institute*, vol. 356, no. 14, pp. 7626–7649, 2019.

[24] D. De Domenico and G. Ricciardi, "Improving the dynamic performance of base-isolated structures via tuned madd damper and inerter devices: A comparative study," *Structural Control and Health Monitoring*, vol. https://doi.org/10.1002/stc.2234, 2018.

[25] P. Deastra, D. Wagg, and N. Sims, "The effect of a tuned-inerter-damper on the seismic response of base-isolated structures," in *16th European Conference on Earthquake Engineering*, 2018.

[26] L. Marian and A. Giaralis, "Optimal design of a novel tuned mass-damperinerter (tmdi) passive vibration control configuration for stochastically support-excited structural systems," *Probabilistic Engineering Mechanics*, vol. 38, pp. 156 – 164, 2014.

[27] M. C. Smith, "Synthesis of mechanical networks the inerter," *IEEE Transactions on Automatic Control*, vol. 47, pp. 1648–1662, Oct 2002.

[28] K. Ikago, K. Saito, and N. Inoue, "Seismic control of single-degree-of-freedom structure using tuned viscous mass damper," *Earthquake Engineering & Structural Dynamics*, vol. 41, no. 3, pp. 453–474, 2012.

[29] V. Lekidis, C. Karakostas, D.G. Talaslidis, "Instrumentation, measurements and numerical analysis of bridges: an example of the cable-stayed bridge on Evripos channel, Greece", *Strong Motion Instrumentation for Civil Engineering*, vol. 373, pp. 481–493, 2001.

[30] V. Lekidis, M. Tsakiri, K. Makra, C. Karakostas, C. Klimis, I. Sous, "Evaluation of dynamic response and local soil effects of the Evripos cable-stayed bridge using multi-sensor monitoring systems", *Engineering Geology*, vol. 79(1-2), pp. 43–59, 2005.

[31] N. Abrahamson, G. Atkinson, D. Boore, Y. Bozorgnia, K. Campbell, B. Chiou, I. Idriss, W. Silva, and R. Youngs, "Comparisons of the nga ground-motion rzelations," *Earthquake Spectra*, vol. 24, no. 1, pp. 45–66, 2008.

[32] D. De Domenico and G. Ricciardi, "Optimal design and seismic performance of tuned mass damper inerter (TMDI) for structures with nonlinear

base isolation systems," *Earthquake Engineering and Structural Dynamics*, vol. 47, no. 12, pp. 2539–2560, DOI: 10.1002/eqe.3098, 2018.

[33] A. Radu, I.F. Lazar and S.A. Neild, "Performancebased seismic design of tuned inerter dampers," *Structural Control and Health Monitoring*, vol. 26, no. 5, https://doi.org/10.1002/stc.2346, 2019.

[34] A. Radu and M. Grigoriu, "An earthquake-source-based metric for seismic fragility analysis," *Bulletin of Earthquake Engineering*, Mar 2018.

[35] M. Grigoriu, "Do seismic intensity measures (IMs) measure up?," *Probabilistic Engineering Mechanics*, vol. 46, pp. 80–93, 2016.

[36] USGS, "U.S. Geological Survey: Uniform hazard tool. last checked on 05/11/2018.," *URL https://earthquake.usgs.gov/hazards/interactive/*, 2018.

[37] A. Papageorgiou and K. Aki, "A specific barrier model for the quantitative description of inhomoeneous faulting and the prediction of strong ground motion. applications of the model," *Bulletin of Seismological Society of America*, vol. 73, no. 4, pp. 953–978, 1983.

[38] A. Papageorgiou and K. Aki, "A specific barrier model for the quantitative description of inhomoeneous faulting and the prediction of strong ground motion. description of the model," *Bulletin of Seismological Society of America*, vol. 73, no. 3, pp. 693–722, 1983.

[39] B. Halldorsson and A. Papageorgiou, "Calibration of the specific barier model to earthquake to different tectonic regions," *Bulletin of Seismological Society of America*, vol. 95, no. 4, pp. 1276–1300, 2005.

[40] A. Radu and M. Grigoriu, "A site-specific seismological model for probabilistic seismic-hazard analysis," *Bulletin of the Seismological Society of America*, vol. 104, no. 6, pp. 3054–3071, 2014.

[41] C. Kafali and M. Grigoriu, "Seismic fragility analysis: Application to simple linear and nonlinear systems," *Earthquake Engineering & Structural Dynamics*, vol. 36, no. 13, pp. 1885–1900, 2007.

[42] A. Radu and M. Grigoriu, "A site-specific ground-motion simulation model: Application for vrancea earthquakes," *Soil Dynamics and Earthquake Engineering*, vol. 111, pp. 77 – 86, 2018.

[43] S. Rezaeian and A. D. Kiureghian, "Simulation of orthogonal horizontal ground motion components for specified earthquake and site characteristics," *Earthquake Engineering & Structural Dynamics*, vol. 41, pp. 335–353, 2 2012.

[44] A. Tsioulou, A. Taflanidis, and C. Galasso, "Modification of stochastic ground motion models for matching target intensity measures," *Earthquake Engineering and Structural Dynamics*, pp. 1–22, 2017.

[45] C. Vlachos, K. G. Papakonstantinou, and G. Deodatis, "Predictive model for site specific simulation of ground motions based on earthquake scenarios," *Earthquake Engineering & Structural Dynamics*, vol. 47, no. 1, pp. 195–218, 2017.

[46] K. Goda, C. Petrone, R. De Risi, and T. Rossetto, "Stochastic coupled simulation of strong motion and tsunami for the 2011 Tohoku, Japan earthquake," *Stochatic Environmental Research and Risk Assessment*, pp. 1–19, 2016.

[47] M. Grigoriu, *Stochastic calculus: Applications in science and engineering.* USA: Birkhäuser, 2002.

[48] G. Deodatis, "Non-stationary stochastic vector processes: seismic ground motion applications," *Probabilistic Engineering Mechanics*, vol. 11, no. 3, pp. 149 – 167, 1996.

[49] R. De Risi, K. Goda, and S. Tesfamariam, "Multi-dimensional damage measure for seismic reliability analysis," *Structural Safety*, vol. 78, pp. 1 – 11, 2019.

[50] D.M. Boore, J.P. Stewart, E. Seyhan, and G.M. Atkinson, "NGA-West2 Equations for Predicting PGA, PGV, and 5% Damped PSA for Shallow Crustal Earthquakes," *Earthquake Spectra*, vol. 30, no. 3, pp. 1057 – 1085, 2014.

[51] T. Thomson, M. Dahleh, "Theory of vibration with applications", *Prentice Hall*, 1993.

[52] D.J. Inman, R.J. Singh, "Engineering Vibration", *Prentice Hall*, 2001.